THE ASTROPHYSICAL JOURNAL, 483:148–160, 1997 July 1
© 1997. The American Astronomical Society. All rights reserved. Printed in U.S.A.

THE INTRINSIC PROPERTIES OF THE STELLAR CLUSTERS IN THE M82 STARBURST COMPLEX: PROPAGATING STAR FORMATION?

S. SATYAPAL,[1,2] DAN M. WATSON,[2] J. L. PIPHER,[2] W. J. FORREST,[2] M. A. GREENHOUSE,[1] H. A. SMITH,[3] J. FISCHER,[4] AND CHARLES E. WOODWARD,[5,6]

Received 1996 July 19; accepted 1997 January 27

ABSTRACT

Near-Infrared spectroscopy combined with high spatial resolution imaging have been used in this work to probe the central 500 pc of M82. Imaging observations in the 2.36 μm CO band head are added to our previously published near-infrared hydrogen recombination line imaging, near-infrared broadband imaging, and 3.29 μm dust feature imaging observations, in order to study the nature of the starburst stellar population. A starburst model is constructed and compared with the observations of the *stellar clusters* in the starburst complex. Our analysis implies that the typical age for the starburst clusters is 10^7 yr. In addition, our high spatial resolution observations indicate that there is an age dispersion within the starburst complex that is correlated with projected distance from the center of the galaxy. The inferred age dispersion is 6×10^6 yr. If the starburst in M82 is propagating outward from the center, this age dispersion corresponds to a velocity of propagation, originating in the center, of ~ 50 km s^{-1}. Our quantitative analysis also reveals that a Salpeter initial mass function, extending from 0.1 to 100 $M_\odot$, can fit the observed properties of M82 without using up more than 30% of the total dynamical mass in the starburst.

Subject headings: galaxies evolution — galaxies: individual (M82) — galaxies nuclei — galaxies: starburst — galaxies: star clusters — infrared: galaxies

1. INTRODUCTION

Numerous galaxies have been observed to be undergoing an intense period of star formation activity that completely dominates the output radiation from the preexisting galaxy. Although there is general agreement on the source for the observed energetic activity in many of these galaxies, fundamental questions on the causes of starburst episodes, their progression and evolution, and the detailed properties of the stars formed in them, are not definitely answered. Efforts to gain a firm understanding of some of these properties will be aided greatly by detailed high spatial resolution observations of nearby starburst galaxies.

M82, close by and hence well studied, has served as the archetypical starburst galaxy, providing an ideal testing ground in which to study starburst theories. In this paper, starburst models are constructed and compared with a series of detailed high spatial resolution near-infrared imaging observations described in depth by Satyapal et al. (1995), hereafter Paper I, and Greenhouse et al. (1997). In Paper I, high spatial resolution near-infrared Fabry-Perot imaging observations of the central kiloparsec of M82, in conjunction with near-infrared broadband imaging observations and imaging in the 3.29 μm dust feature, were used to examine the extinction toward the starburst region, the state of the ionized gas, and the nature of the stellar population.

In this article, we conduct a quantitative analysis of the major points discussed in Paper I. In addition, new imaging observations of the 2.3 μm CO absorption feature are added to our previously published results, providing further insight into the starburst episode in M82. Unlike most past studies of M82, we model the properties of the individual *stellar clusters* in the central 500 pc region.

In the next section, we describe our new CO band head observations of M82, and the results are presented in § 3. The stellar clusters within the central 500 pc are identified, and their major intrinsic properties are summarized in § 4. Our starburst model is described in § 5 and is applied to the stellar clusters in M82 in § 6.

2. CO 2.3 μm ABSORPTION FEATURE OBSERVATIONS

2.1. *Background*

Observations of the first-overtone bands of CO near 2.3 μm have been used widely to probe the stellar population in galaxies. This feature, observed only from the atmospheres of cool stars, shows a systematic increase in depth with increasing stellar luminosity and decreasing effective temperature (Frogel et al. 1978, hereafter F78; Kleinmann & Hall 1986). It is also found to increase with increasing metallicity (Frogel, Persson, & Cohen 1983). The strength of the feature is defined by the "CO index," which is essentially the difference in magnitudes between the center of the CO obsorption and the extrapolated continuum.

Observers have used a variety of spectral resolutions and wavelengths to measure the CO index. In the early work on CO indices by F78, the stellar CO absorption feature was characterized using the "photometric CO index," CO_F, defined as the difference in magnitudes between the narrow-band filters centered at 2.2 μm ($\Delta\lambda = 0.11$ μm) and 2.36 μm ($\Delta\lambda = 0.08$ μm) relative to the star α Lyrae. Unlike these measurements, our present observations ($\Delta\lambda = 0.04$ μm) permit the measurement of the slope of the continuum,

[1] Goddard Space Flight Center, Code 685, Greenbelt, MD 20771.
[2] Department of Physics and Astronomy, University of Rochester, Rochester, NY 14627-0011.
[3] Harvard-Smithsonian Center for Astrophysics, 60 Garden Street, Cambridge, MA 02138.
[4] Remote Sensing Division, Naval Research Laboratory, Code 7600, 4555 Overlook Avenue, SW, Washington, DC 20375.
[5] Department of Physics and Astronomy, University of Wyoming, Laramie, WY 82071-3905.
[6] NSF Presidential Faculty Fellow.

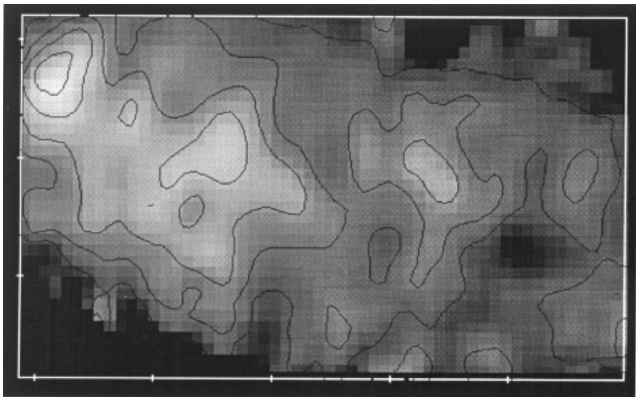

FIG. 1*a*

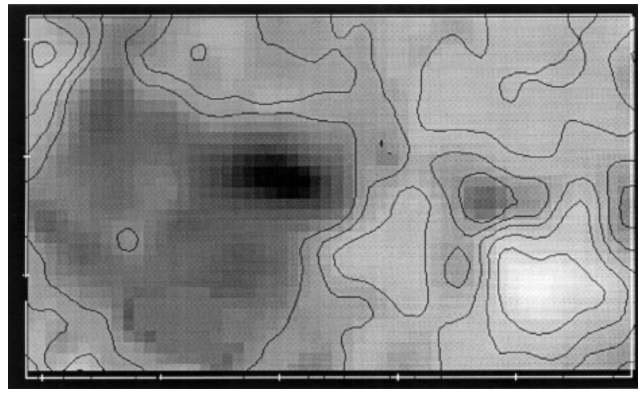

FIG. 1*b*

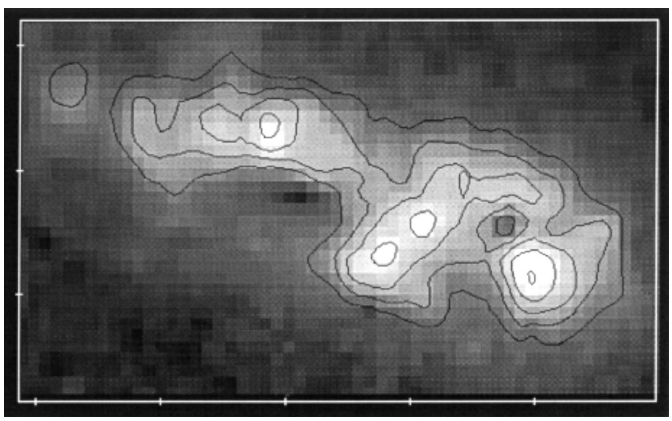

FIG. 1*c*

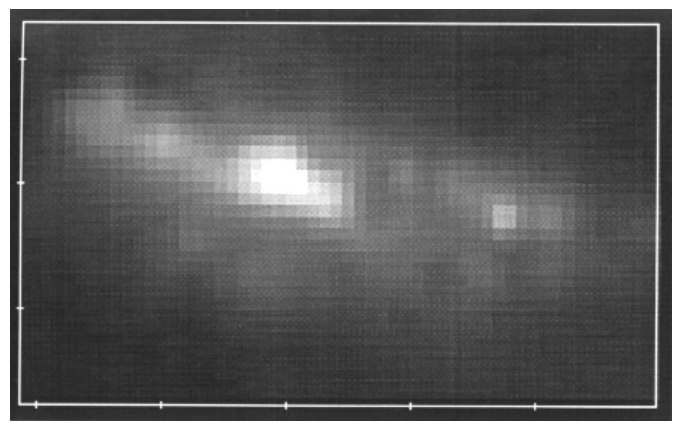

FIG. 1*d*

FIG. 1.—2.36 μm CO absorption distribution compared with the Brγ emission in M82. (*a*) CO index image with contours overlaid. Contours displayed from 0.1 to 0.3 arcsec^{-2} in intervals of 0.05 arcsec^{-2}. Tick marks correspond to 5″. North is up, and east is to the left. (*b*) W(Brγ) image with contours overlaid. Contours displayed from 1.5 to 2.0 arcsec^{-2} in intervals of 0.1 arcsec^{-2}. (*c*) Brγ image with contours overlaid. Contours displayed from 1.5×10^{-17} to 3×10^{-17} W m^{-2} arcsec^{-2} in intervals of 5×10^{-18} W m^{-2} arcsec^{-2} (*d*) K-band image.

allowing any necessary correction for deviations from a flat continuum, e.g., reddening. In addition, the higher resolution observations allow us to choose wavelengths that avoid contamination of the measured flux from strong emission lines that may be present in the spectrum of objects such as M82 (e.g., Brγ; $\lambda = 2.166$ μm).

Observations of the CO index in the dust-enshrouded nuclei of starburst galaxies can serve as a powerful tool in the study of the late-type stellar population. It has the advantage of being, in principle, independent of extinction, mass, and distance and can thus provide potentially an observationally rigid constraint to models of the starburst population.

2.2. CO *Band Head Images of M82*: *Observations and Data Reduction*

The CO band head observations of M82 were carried out in 1995 June at the Wyoming Infrared Observatory (WIRO) with the university of Rochester Third Generation Array Camera using the 1.85% bandwidth cold circular variable filter (CVF). Images were taken with the CVF set to 2.140, 2.250, and 2.360 μm. Ten 20 s on-source integrations and 10 background integrations at each of these wavelength settings were obtained. On-chip nodding was used to double our efficiency. The plate scale was 0″.24 pixel^{-1}, and the spatial resolution was 1″.2. The wavelengths were chosen after examining a high-resolution spectrum of an M5 III star from the Kleinmann & Hall (1986) stellar atlas and optimizing on the depth of the absorption feature for our spectral resolution. The continuum settings were selected to measure the slope accurately and to ensure that these wavelengths were not near emission lines that would be present in M82. A standard star with no CO absorption in its spectrum was chosen as a flux calibrator (ν UMa; F2 IV, $m_K =$ 2.99). The two continuum images were used to determine the extrapolated continuum at 2.36 μm, and an image of the CO index was generated. Using an electronic version of the Kleinmann & Hall (1986) stellar atlas, the CO index was calculated synthetically using our spectral resolution and choice of wavelengths and using those of F78, and the results were compared. Our present CO index was found to be roughly consistent with J. A. Frogel's; the relationship between the two is given by

$$\mathrm{CO}_F = 1.127\ \mathrm{CO}_{\mathrm{this\ work}} - 0.004\ . \qquad (1)$$

3. DISTRIBUTION OF THE 2.36 μm CO ABSORPTION FEATURE IN M82

Normal galaxies have typical CO indices of 0.15, with very little scatter around this value (F78). Deeper absorption depths in galaxies can be produced by a large population of late-type supergiants and massive giants, or by a metal-enriched, otherwise normal population of stars. Shallower depths can be produced by an enhanced population of early-type stars or by the contamination of the K-band

continuum from nonstellar processes (e.g., free-free and free-bound emission from ionized gas, and the emission from hot dust). The image of the CO index of M82, together with our Brγ image (Paper I), and our image of the Brγ equivalent width, W(Brγ), are shown in Figure 1. A K-band image is also displayed for comparison. The CO index ranges from $\sim$0.26 in individual pixels to $\sim$0 across the central 500 pc. As can be seen in Figure 1, the CO index is distinctly anticorrelated with the Brγ equivalent width in M82; the CO index is high at the nucleus where W(Brγ) is low and is at its minimum $\sim$12″ west and 3″ south of the nucleus where W(Brγ) is at its maximum. Since the Brγ emission is tracing both the bluest stellar population and the regions where the contribution to the K-band continuum from nebular and dust emission is highest, this anticorrelation is expected.

4. INTRINSIC PROPERTIES OF THE STELLAR CLUSTERS

In this section, we summarize the major properties of the stellar clusters found in the central 500 pc of M82. In order to determine the intrinsic properties of the stellar clusters in the M82 starburst, an extinction correction must be applied to the observed emission. In Paper I, we used an extinction map that was generated using the observed Paβ/Brγ flux ratio, assuming case B recombination, and the $\tau_\lambda \propto \lambda^{-1.85}$ (Landini et al. 1984) extinction law to deredden the broadband images, generating extinction-corrected J, H, and K images. We also calculated the free-free and free-bound components of the broadband emission in an effort to separate out the stellar component.

4.1. *Identification of Pointlike Sources*

The extinction-corrected K-band image was used to search for pointlike sources using the task DAOFIND in the DAOPHOT software package (Stetson 1987). This algorithm searches for local maxima in the input image whose amplitudes are greater than a user-specified detection threshold. Twelve pointlike sources were identified and are displayed in Figure 2, and their positions are given in Table 1. Based on their luminosity and spatial extent (Table 2) at the distance of M82, these pointlike sources are likely to be young compact star clusters. In order to determine the properties of these clusters, 2″ diameter circular apertures were centered on each of the 12 sources, and standard aperture photometry was carried out at these positions. Initial attempts to extract the magnitudes of these pointlike sources involved experimenting with PSF-fitting algorithms in the DAOPHOT software package. However, these algorithms are optimized for crowded stellar field photometry

TABLE 1

POSITIONS OF THE 12 POINTLIKE BROADBAND NEAR-INFRARED SOURCES IDENTIFIED IN THE CENTRAL 500 pc OF M82

Source Number	Right Ascension Offset[a]	Declination Offset[a]
1	−6.7	2.6
2	−4.6	1.4
3	−3.5	−2.6
4	0.0	0.0
5	3.8	−2.6
6	5.0	−0.1
7	7.1	−0.6
8	0.4	−3.9
9	0.9	−1.7
10	10.8	−3.5
11	10.9	−1.8
12	13.2	−3.4

[a] Offsets from K nucleus in arcseconds. Eight of the sources correspond to sources identified by Pipher et al. 1987

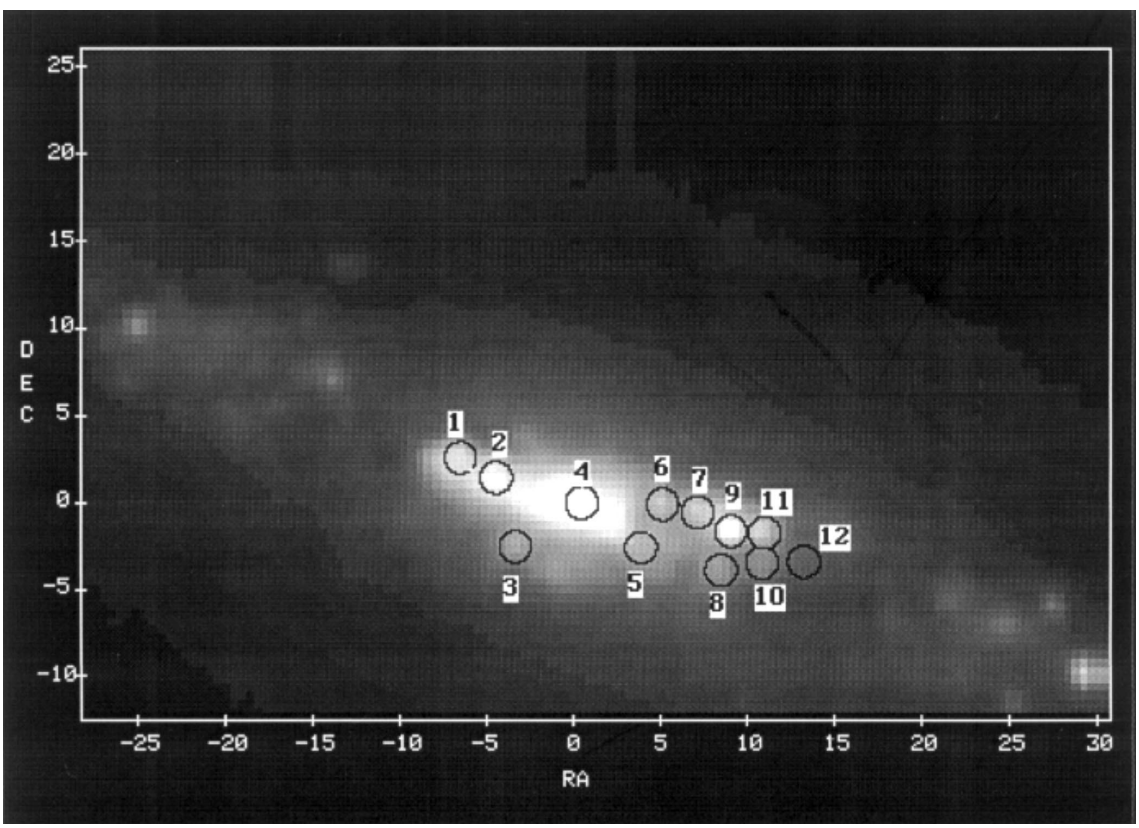

FIG. 2.—Pointlike sources in the central 500 pc of M82. Foreground extinction-corrected K-band image with the location of the 12 compact objects. North is up, and east is to the left; (0, 0) corresponds to the position of the nucleus.

TABLE 2

SUMMARY OF PROPERTIES OF POINTLIKE SOURCES IN M82

Source	$m_K^{\rm uncor}$	$m_K^{\rm cor}$	$(J-H)_{\rm uncor}$	$(H-K)_{\rm uncor}$	$(J-H)_{\rm cor}$	$(H-K)_{\rm cor}$	$J_{\rm ff+fb}$ (%)	$H_{\rm ff+fb}$ (%)	$K_{\rm ff+fb}$ (%)	$J_{\rm bb}$ (%)	$K_{\rm bb}$ (%)	$K_{\rm dust}$ (%)
1	10.8[a]	10.1[a]	1.03[b]	0.77[b]	0.17[b]	0.20[b]	1[c]	2[c]	3[c]	1[d]	1[d]	13[e]
2	10.6	10.0	1.02	0.72	0.28	0.21	2	2	3	1	1	12
3	11.3	11.0	0.89	0.55	0.47	0.28	2	2	3	1	1	13
4	9.9	9.3	1.40	0.91	0.53	0.37	1	1	1	1	0	20
5	11.1	10.1	1.35	0.94	0.30	0.27	4	4	6	2	1	15
6	11.1	10.2	1.31	0.87	0.28	0.24	3	3	5	2	1	13
7	11.0	10.2	1.04	0.71	0.14	0.13	3	3	6	2	1	7
8	11.4	10.7	1.23	0.82	0.41	0.28	4	4	6	3	1	13
9	10.7	10.0	1.10	0.80	0.31	0.31	2	2	4	1	1	19
10.....	11.5	10.7	1.23	1.01	0.27	0.39	7	7	11	4	2	24
11.....	11.0	10.3	1.14	0.80	0.37	0.33	3	3	5	2	1	18
12.....	12.0	11.2	1.26	1.03	0.35	0.44	8	7	11	5	2	26

[a] We estimate a 10% error in our photometry. All quantities correspond to a 2″ aperture centered on specified source.

[b] The estimated error in our colors is 15%. The corrected colors correspond to extinction-corrected values. The free-free and free-bound components were subtracted out.

[c] The percent contribution from free-free and free-bound processes at the indicated bandpass.

[d] The percent contribution from the Paβ and Brγ line flux to the broadband continuum.

[e] The fraction of the K-band continuum from thermal emission from 600 K dust required to generate "normal" colors (see Fig. 3).

with minimal overlying nebulosity. When using these algorithms on the extinction-corrected K-band image of M82, the combination of luminous and variable nebulosity, crowded field photometry, and the lack of isolated, pure point sources needed to characterize the point-spread function (PSF) resulted in unsuccessful point-source subtractions. We therefore used standard aperture photometry on our images, with apertures that were small enough to prevent overlap among the pointlike sources (see Fig. 2). The flux in these apertures was taken to represent the total flux from the stars in the clusters, the emission from the ionized gas, and dust emission. In reality, there can be some small contribution to the continuum emission from the underlying old stellar population; a component of the total ionized gas could be ionized from the background interstellar radiation field and not entirely by the stars from that cluster, and there could be a contamination to the total emission from one source from its neighboring sources.

4.3. *Summary of Intrinsic Properties of Pointlike Sources*

Using a foreground screen extinction model, the observed magnitudes and colors of each of the point sources were corrected for extinction, and the components to the near-infrared emission described in Paper I were calculated. The results are summarized in Table 2. In addition to the free-free and free-bound components to the broadband continuum, the contributions to the broadband emission from the Paβ and Brγ line flux were also calculated. The spectrum of M82 includes many other emission lines, but they do not comprise a significant component of the broadband emission; the maximum contribution to the J-band continuum from the Paβ line flux is 5%.

Table 3 summarizes various other properties of the 12 pointlike sources. The extinction-corrected Brγ line flux was used to calculate the number of $O4$ V stars (Panagia 1973) required to produce this flux; the emission from these stars

TABLE 3

SUMMARY OF PROPERTIES OF POINTLIKE SOURCES IN M82 CONTINUED

Source	$F_{\rm Br\gamma}^{\rm cor}$ (10^{-17} W m^{-2})	$N_{\rm UV}$ (s^{-1})	$N_{\rm O4\,V}$	log [W(Brγ) (A)]	$\rm CO_{observed}$	$\rm CO_{intrinsic}$
1	7.9[a]	6.1	71[b]	1.295[c]	0.172[d]	0.177[e]
2	10.5	8.0	94	1.357	0.206	0.214
3	3.7	2.8	33	1.311	0.142	0.147
4	8.1	6.2	73	0.977	0.215	0.219
5	17.0	13.1	153	1.637	0.113	0.121
6	12.9	9.9	117	1.532	0.208	0.221
7	15.1	11.6	136	1.597	0.243	0.261
8	10.6	8.1	96	1.636	0.154	0.165
9	10.7	8.2	96	1.363	0.191	0.199
10.....	18.4	14.1	166	1.882	0.129	0.146
11.....	11.6	8.9	105	1.536	0.044	0.047
12.....	11.2	8.6	101	1.863	0.157	0.177

[a] We estimate a 10% error in our photometry. All quantities correspond to a 2″ aperture centered on specified source.

[b] The number of O4 V stars was calculated using the ionizing photon rates from Panagia 1973.

[c] ± 0.01.

[d] The estimated uncertainty is 0.015.

[e] The intrinsic CO index was calculated by diluting the feature depth by the free-free and free-bound processes listed in Table 2.

in the K band was found to contribute less than 1% to the total K-band continuum at each of the sources. The observed CO indices of each of the sources, along with the values corrected for the free-free and free-bound continuum, are also listed in Table 3.

The observed and corrected colors of the 12 sources are shown in Figure 3. Vectors indicating the effects of foreground extinction, extinction from a uniform mixture of dust and stars, and the emission from 600 K dust are also shown. The colors have been corrected for foreground extinction, and the free-free and free-bound components were removed (see Paper I). As can be seen from Figure 3, the sources have corrected colors that are significantly different from those of normal stars or clusters of normal stars. All have $H-K$ colors that are "too red" relative to their corresponding $J-H$ color. Many starburst galaxies have colors that occupy this region of the color-color diagram (see Doyon, Joseph, & Wright 1994; Turner 1995; Satyapal 1995; Smith et al. 1996). If we assume that the position of these sources on the two-color diagram can be ascribed to the emission from a normal population of stars and the emission from dust, we can calculate the fraction of the broadband emission attributable to dust emission. This fraction is listed in Table 2. The dust emission was modeled by graybody dust grains with emissivity $\epsilon \propto \lambda^{-2}$ (see Aaronson 1977) and a temperature of 600 K. However, under this assumption, the dust dilutes the CO index, and the resulting relatively blue colors of the stellar clusters are generally inconsistent with their CO indices (see Table 2) for any normal population of stars. The CO index corresponding to the $J-H$ colors of normal supergiant stars is displayed on the right axis in Figure 3. Thus, we conclude that in order for the corrected colors to be consistent with the observed CO indices, a combination of purely foreground extinction and dust emission cannot be the only effects considered.

4.4. *Effects of Different Models of the Dust Geometry*

In the previous section, we have shown that a purely foreground extinction screen does not result in extinction-corrected colors that are consistent with normal stellar populations and that dust emission cannot be invoked. In this section, we investigate the effects of varying the assumed dust geometry on the extinction-corrected colors (assuming no dust emission). For the purpose of illustrating the importance of these effects on near-infrared colors in general, we will use the integrated colors from a large aperture centered on the M82 nucleus as representative.

In this section, we will consider three different dust geometries, all considered previously in the study of M82 (e.g., McLeod et al. 1993; Puxley 1991; Telesco et al. 1991). The first is the simple foreground screen geometry discussed above. Here the ionized gas, toward which the extinction is calculated, and the stars are being obscured by a single overlying screen. The second is a homogeneous mixture of stars, gas, and dust. Finally, we will consider a two-screen geometry, where the ionized gas and stars are being obscured by a dust screen, followed by another emission region of stars and gas emitting a fraction of the first emitting region's intensity, followed by another dust screen.

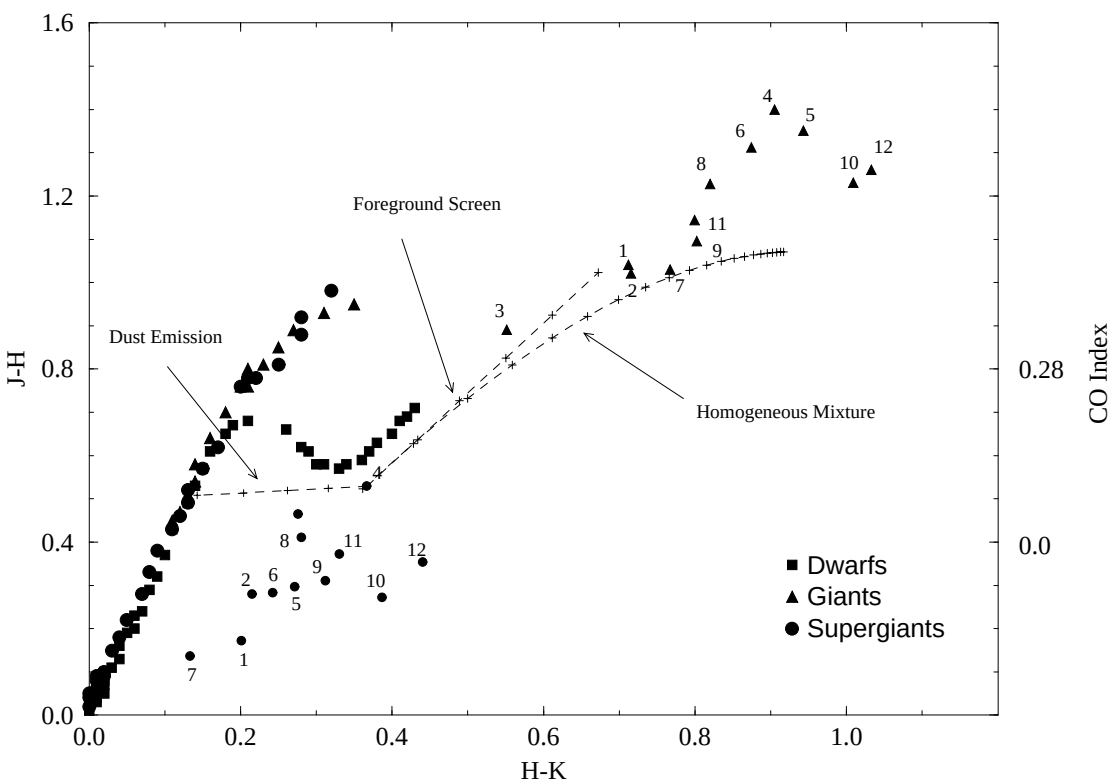

FIG. 3.—Two-color diagram of the M82 pointlike sources. The filled triangles correspond to the observed colors, while the filled circles correspond to the corrected colors. The colors have been corrected using the foreground screen-derived recombination line extinction map, and the free-free and free-bound components to the broadband emission have been removed. The three dashed lines correspond to the effects of foreground extinction, a homogeneous mixture extinction geometry, and the thermal emission from 600 K dust. The tick marks on the reddening vectors correspond to τ_K of 0.2. The tick marks on the dust emission vector correspond to 5% fractions of the total K flux density. The colors of normal stars are also shown in the figure (Koornneef 1983). The CO index of normal supergiants is indicated on the right axis (F78).

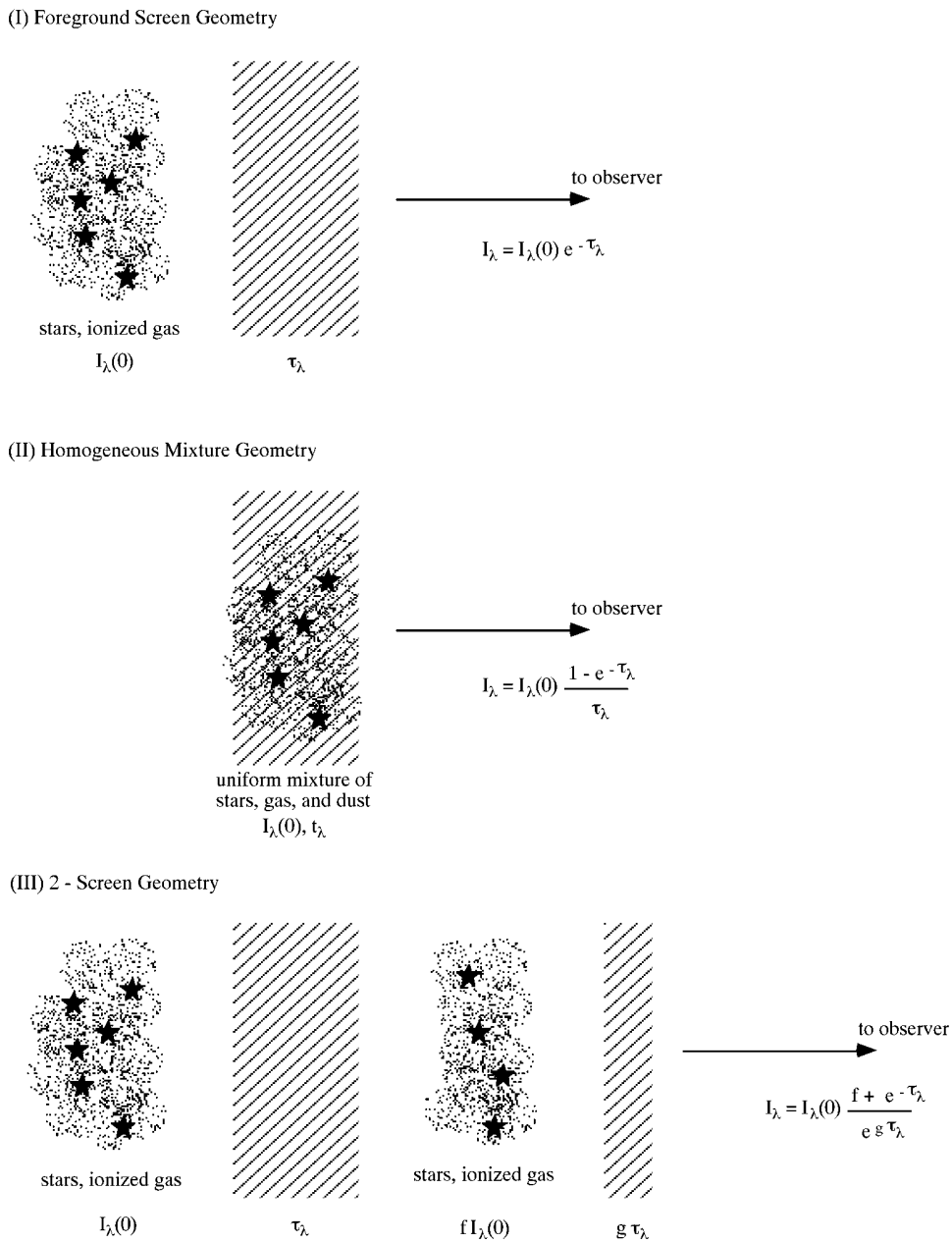

FIG. 4.—Different dust geometries

These geometries are illustrated in Figure 4.[7] The resulting colors are shown on a color-color diagram in Figure 5. We have used the integrated emission from a 24″ aperture centered on the nucleus. The extinction was then calculated for each of the discussed dust geometries using the total Brγ and Paβ line fluxes in this aperture ($F_{\mathrm{Br}\gamma} = 4.24 \times 10^{-15}$ W m^{-2} and $F_{\mathrm{Pa}\beta} = 9.35 \times 10^{-15}$ W m^{-2}), adopting the same assumptions of case B recombination discussed earlier (Paper I). An extinction power law, $\tau_\lambda \propto \lambda^{-1.85}$, was again employed. The resulting values for τ_K and the extinction-corrected K-band magnitudes are also shown in Figure 5. In addition, we have calculated the CO index, also displayed in Figure 5, from the integrated flux densities at 2.36, 2.25, and 2.14 μm in a 24″ aperture. As can be seen from Figure 5, the assumed dust geometry has a significant effect on the corrected colors. A foreground screen geometry does *not* generate corrected colors that are consistent with the colors of any normal stars. However, a first-order correction to the foreground screen geometry, namely, the two-screen geometry with $f = 0.3$ and $g = 0.2$, can generate corrected colors characteristic of normal stars that are consistent with the observed CO index of 0.18. Although these two models generate significantly different colors, the extinction-corrected K-band magnitudes are not appreciably different. The difference between the corrected magnitudes in these two cases is only 0.24, or a factor of 1.2 in the corrected K-band luminosities. Thus, a small variation of the foreground screen geometry can have a substantial effect on the extinction-corrected colors of the M82 starburst without significantly affecting the corrected magnitudes. Note that the extinction model must result in

[7] Adapted from McLeod et al. (1993).

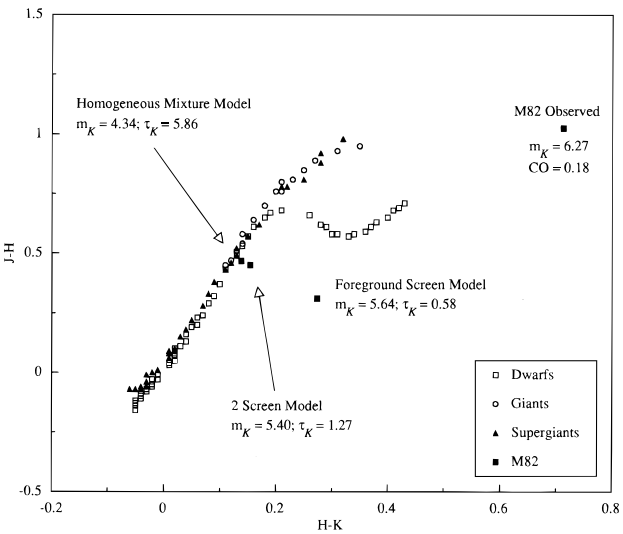

FIG. 5.—Two-color diagram of the representative colors of the M82 starburst. The effects of different dust geometries on the corrected colors are indicated. Values for τ_K and m_K (before and after extinction corrections have been applied) are indicated. The average value for the CO index is also shown.

"normal" colors without changing substantially the derived corrected magnitudes from their corresponding foreground screen values. As mentioned in Paper I, the extinction-corrected Brγ flux cannot overpredict the thermal bremsstrahlung continuum at millimeter wavelengths. Using our foreground screen extinction-corrected Brγ image, the total extinction-corrected flux of 1.0×10^{-14} W m^{-2} results (assuming case B recombination, $T_e = 5000$ K) in a derived 3 mm free-free continuum flux density that is already $\sim$75% of that observed (Carlstrom & Kronberg 1991). Since the emission at 3 mm has some nonthermal component as well as a component from dust, the extinction-corrected Brγ flux cannot be much larger than that obtained using our foreground screen extinction model. Thus, although we cannot constrain precisely the extinction geometry, we can say that the extinction model must result in "normal" colors and, at the same time, cannot produce corrected magnitudes substantially different from those obtained using a foreground screen extinction model. With only two recombination line maps, however, we cannot constrain the extinction geometry more precisely. In order to obtain more meaningful extinction-corrected colors for the stellar clusters in the M82 starburst, at least one additional recombination line image would be required. For example, imaging in the Brα (4.05 μm) line would allow us to conduct a more rigorous study of the extinction in the M82 starburst, resulting in colors that would be more representative of the true colors of the central stellar clusters.

The analysis above emphasizes the need to exercise caution in interpreting extinction-corrected colors. For the case of M82, we have confirmed a *predominantly foreground* screen model for the extinction, but we have shown that a slight deviation from this extinction model can affect the corrected colors significantly. The corrected magnitudes, however, are not affected substantially. Hence, all extinction-corrected absolute quantities are well determined in our study of M82. The extinction-corrected colors, however, are not determined precisely enough for comparison with stellar population models, for which very small color changes are significant.

5. STARBURST MODEL

In order to conduct a quantitative investigation of the properties of the starburst clusters in M82, we have constructed our own set of population synthesis models. Unlike most previous studies of starburst galaxies, our models can be applied not only to the integrated properties of a starburst, but, in the case of M82, to the observations of the individual *stellar clusters*.

Our model is analytic and assumes a power-law initial mass function (IMF) between a variable lower mass cutoff and a fixed upper mass cutoff of $m_U = 100\ M_\odot$. The other free parameter in the model is the total mass assumed in the burst. As an illustrative case, we have assumed a single IMF slope set at the Salpeter value for the solar neighborhood of $\Gamma = 1.35$ (Salpeter 1955). More recent studies of the solar neighborhood IMF have shown that the low-mass IMF is nearly flat (e.g., Bessell & Stringfellow 1993) while the high-mass IMF for field stars is steeper than the Salpeter value (e.g., Massey et al. 1995b), although the cluster IMF for high-mass stars in the solar neighborhood is similar to the Salpeter IMF (Massey, Johnson, & De Gioia-Eastwood 1995a). We have taken this simple case to illustrate the relationship between the observed quantities and the parameters derived for the IMF. The stellar tracks for solar metallicity stars ($Z = 0.02$) by Schaller et al. (1992) were used. We have also assumed an instantaneous burst of star formation. In reality, the star formation rate in a starburst galaxy nucleus can have a complicated time dependence. However, unlike previous studies of M82, we are modeling the *stellar clusters* in the M82 starburst that are characterized more accurately as "instantaneous starbursts" than are the integrated properties from the entire starburst region. We have synthesized the J, H, and K magnitudes and colors, the supernova rate, and the CO index for a starburst population with ages ranging from 10^5 to 10^8 yr. The CO index was calculated using the analytical expressions from Doyon et al. (1994). The Brγ equivalent width, W(Brγ), from Leitherer & Heckman (1995) was compared with our data also. We do not include the effects of a nebular continuum or a preexisting population of stars. Our data permit us to subtract the nebular continuum, allowing direct comparison with the model quantities. The preexisting stellar population does not contribute significantly to the total luminosity from the central 30″ of M82. The total foreground extinction-corrected K-band magnitude in a 30″ aperture centered on the nucleus is -22.0. Assuming that the mass–to–K-band luminosity ratio of the old stellar population is comparable to the value of 23 $M_\odot/L_\odot$ observed in normal galactic bulges (Devereux, Becklin, & Scoville 1987; Thronson & Greenhouse 1988; Gaffney, Lester, & Telesco 1993), the old stars would have an absolute K-band magnitude of -18.1, or 3% of the total extinction-corrected K-band luminosity, if they constituted 50% ($3.5 \times 10^8\ M_\odot$) of the total dynamical mass within the central 450 pc. The results of our model were found to be well within the range obtained by other models (e.g., Leitherer & Heckman 1995; Charlot & Bruzual 1991).

The calculated quantities described above can be used to constrain the age and IMF of a starburst when compared with observations. We now compare the model predictions with the starburst episode in M82.

6. APPLICATION TO M82

6.1. *Age of the Burst: Propagating Star Formation?*

Several observations suggest that the starburst is propagating outward from the center of M82. The K-band emission, presumably dominated by the output from evolved stars, is relatively smooth and centrally concentrated (see Fig. 2), while the recombination line (Paper I), 10 μm (Telesco et al. 1991), and 3.29 μm dust feature (Paper I) emission show a more bilobal distribution. This suggests that the nucleus contains an older stellar population and that the starburst may be propagating outward. In Paper I, the radial variation in the 3.29 μm dust feature–to–Brγ flux ratio was shown to provide additional qualitative evidence for the presence of a radially dependent age variation in the central 500 pc. Since the 3.29 μm dust feature is thought to be the result of nonequilibrium heating of small grains by ionizing and lower energy photons, while the Brγ emission is related only to ionizing photons, the variation of the extinction-corrected ratio from values greater than 35 near the nucleus to 6 at the position 15″ west of the nucleus may be a crude indicator of the hardness of the radiation field within the starburst region, again suggesting a radially dependent evolutionary effect. In this section, a more quantitative investigation of the age of the starburst complex using our starburst models will be carried out.

The age of the stellar clusters within the M82 starburst can be inferred most accurately by the observed CO index and W(Brγ), as has been done previously for other starburst galaxies (e.g., Doyon et al. 1994). These observations are particularly well suited to constraining the age of a stellar population since the model quantities show a sharp change in a short time interval. The evolution of the CO index and W(Brγ) for a starburst model with $m_L = 1\ M_\odot$ and $m_U = 100\ M_\odot$, together with the observed values at the positions of the 12 pointlike sources discussed in § 4, is shown in Figure 6. These model quantities are relatively insensitive to the lower mass cutoff assumed and thus can be used to derive the age of the starburst independently. The observed values have not been corrected for dust emission or the small continuum contribution from an old stellar population. These components would not have a substantial effect on the CO index or much less the Brγ equivalent width. The CO indices imply ages between 4×10^6 and 1×10^7 yr for the 12 different sources, roughly consistent with the ages inferred from the observed Brγ equivalent widths. Although the precise age depends on the detailed time dependence of the star formation rate, the observed CO indices and Brγ equivalent widths imply a relatively narrow range in age (the effects of these model quantities on the assumed star formation rate can be found in Doyon et al. 1994). Thus, the implied age for the M82 starburst is approximately 10^7 yr. The most recent estimate of the age of the starburst in M82 by Rieke et al. (1993) is (1.3–3) $\times 10^7$ yr, depending on the details of the assumed star formation rate. Their model of the integrated emission from the central $\sim$500 pc required incorporation of two bursts. We have obtained estimates of the age of the *stellar clusters* directly. At these times, the most massive stars have completed nuclear burning, and the effective temperature of the ionizing stars is $\sim$35,000 K, consistent with estimates derived from various forbidden line ratios (e.g., Achtermann & Lacy 1995). Early starburst models imposed an upper mass cutoff to account for the relatively soft radiation field; since the effective temperature of the ionizing stars decreases naturally with time as the most massive stars evolve off the main sequence, this assumption is not necessary.

Apart from determining the age of the M82 starburst as a whole, our high spatial resolution data, together with our starburst models, allow a quantitative investigation of the possible radial age gradient. In this scenario, star formation, which initially started at the nucleus, induces star formation at other locations as the newly formed population of stars compress the surrounding regions. With Figure 6, we can estimate the age dispersion implied by the observed W(Brγ) and CO index within the central $\sim$500 pc. The estimated age dispersion obtained through the spread in CO indices of the 12 different sources is $\sim 6 \times 10^6$ yr. The maximum projected separation is $\sim$230 pc, implying a velocity of propagation, originating in the center, of 40 km s^{-1}. Using the spread in the values of W(Brγ), the inferred velocity is 60 km s^{-1}. This velocity is not an unreasonable velocity for expansion. Achtermann & Lacy (1995) find evidence for radial expansion of the ionized gas at $\sim$55 km s^{-1} from the nucleus of M82. The correlation between the CO index and W(Brγ) for the 12 pointlike sources is shown in Figure 7.

The dependence of the CO index and the Brγ equivalent

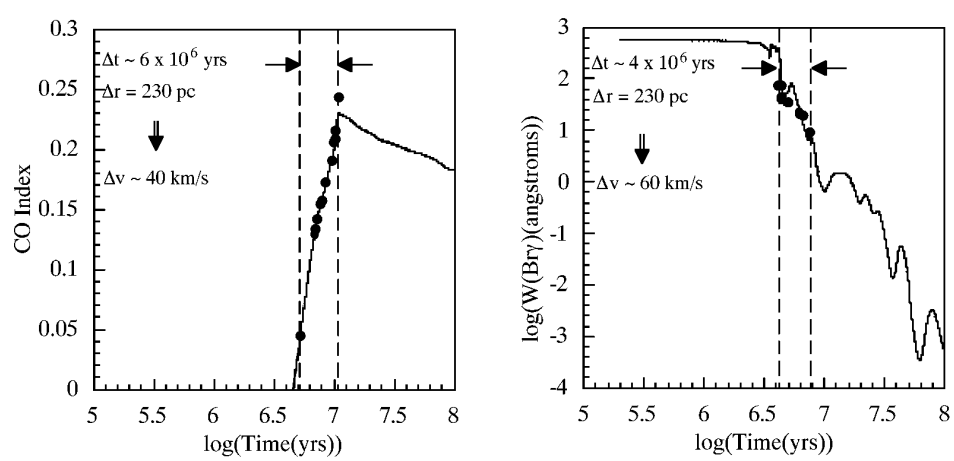

FIG. 6.—The CO index as a function of time for a starburst model with $m_L = 1\ M_\odot$ and $m_U = 100\ M_\odot$, together with the intersections of the observed values of the 12 pointlike sources.

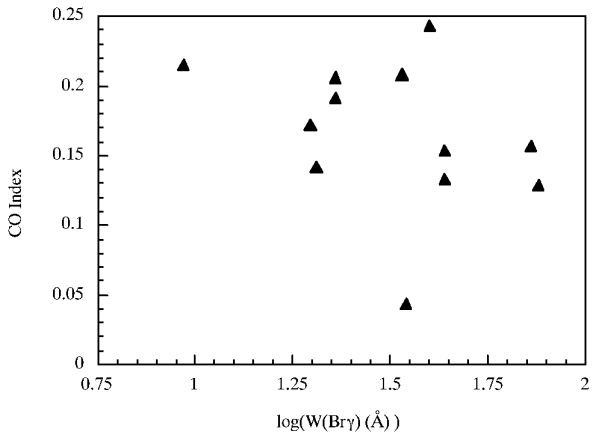

FIG. 7.—CO index vs. W(Brγ) for the 12 pointlike sources

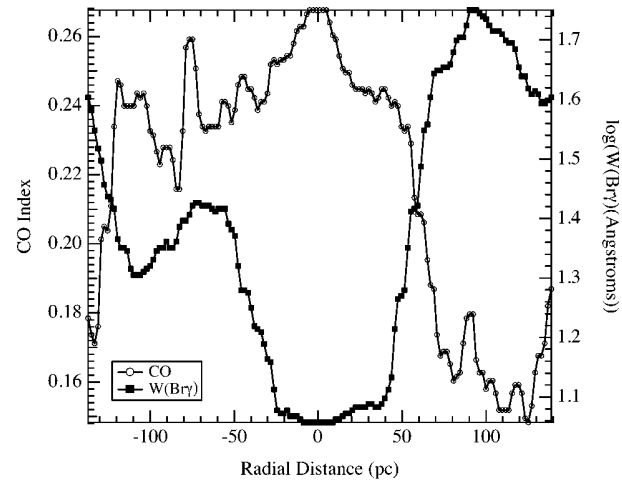

FIG. 9.—CO index and W(Brγ) along the major axis of the galaxy

width on the projected radius for the 12 different pointlike sources is shown in Figure 8. There is a general anticorrelation of the CO index with the Brγ equivalent width as a function of projected radius; radii close to the nucleus are generally associated with larger CO indices and lower Brγ equivalent widths, while the opposite situation prevails at larger radii. This anticorrelation is most pronounced along the major axis of the galaxy, as can be seen in Figure 9. It should be noted that the decrease in the CO index with radius is not the result of the "filling in" of the absorption feature with increasing nonstellar continuum, as can be seen from Figure 10. In addition to correcting the CO index for dilution from the nebular component discussed in § 4.3 and Paper I, the dilution resulting from "hot" dust emission was also estimated. The near-infrared emission from a collection of small particles transiently heated by the absorption of ultraviolet and visible photons resembles that of a graybody with color temperature 1000 K (Sellgren, Werner, & Dinnerstein 1983). Sellgren et al. have shown that the 3.29 μm line–to–continuum ratio is roughly constant at several locations in a number of reflection nebulae. Using this constant ratio of ~ 6, the extinction-corrected 3.29 μm feature image, and the assumption that the hot dust continuum can be approximated by a 1000 K graybody, the extinction-corrected flux density from hot dust emission near 2 μm was calculated and accounted for in the CO index image. Source 7 appears to have an anomalously high CO index compared with its Brγ equivalent width. We note that our CO band head and Brγ data were obtained using the same telescope and camera, and the data were reduced consistently.[8] Our measured CO index at the position of the nucleus using the appropriate apertures was found to be in good agreement with that found by McLeod et al. (1993) and Lester et al. (1990). The scatter in the CO index versus the W(Brγ) graph is therefore not a reflection of the observational uncertainty of our data. The high CO index of source 7 may be due to a higher metallicity in this source, although the required metallicity would be extreme. Using the calibration derived from the observations of globular clusters (Frogel et al. 1983), if the observed CO index of 0.24 in source 7 is the result of a metal-enriched population of

[8] Error bars for these quantities are displayed in Fig. 8 and listed in Table 3.

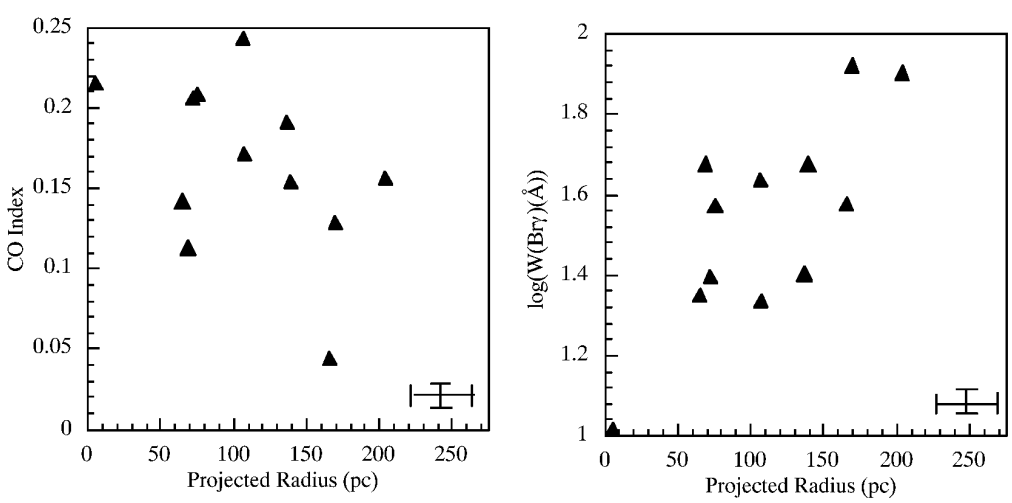

FIG. 8.—*Left panel*: CO index for the 12 different sources, identified by number, vs. projected radius from the nucleus. The estimated uncertainty in the CO index is shown in the lower right-hand corner. *Right panel*: W(Brγ) vs. projected radius. The estimated uncertainty is shown in the lower right-hand corner.

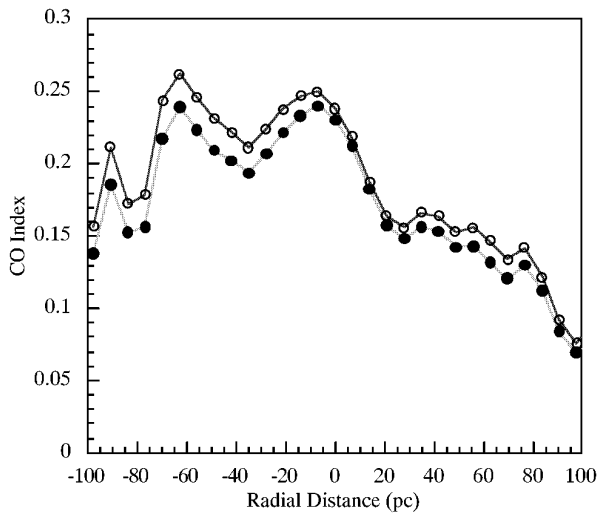

FIG. 10.—Radial variation of the observed (*filled circles*) and intrinsic (*open circles*) CO index along the major axis of M82. The intrinsic CO index was calculated by removing the effects of the free-free, free-bound, and hot dust emission near 2 μm. An estimate of the hot dust emission, calculated by using the 3.29 μm feature flux, and the assumption of a line–to–hot dust continuum ratio of 6 (Sellgren et al. 1983), was also subtracted out.

otherwise normal giants, the metallicity would have to be a factor of ~ 12 larger than solar (CO = 0.16 + 0.074[Fe/H], where [Fe/H] is the logarithm of the metal abundance relative to solar; Frogel et al. 1983). The metallicity dependence of the CO index was determined from data on globular cluster giants with below solar abundances; the reliability of this calibration for the present data is therefore unknown. Although the correlation is not remarkable, these data suggest, most importantly, that there is an age dispersion within the starburst region of M82, and that this age dispersion appears to be correlated generally with projected radius. Most previous starburst models have treated the integrated quantities within the inner ~ 450 pc as a single burst. Rieke et al. (1993) approximated the continuum of starburst activity by two bursts in their models in order to account for roughly two characteristic populations—a young blue one farther from the nucleus and an older, redder nuclear population. As we have seen, there is a continuum of starburst activity possibly moving outward, probably as a result of sequential star formation.

6.2. *Is the IMF Deficient in Low-Mass Stars?*

Our extinction corrections (Paper I) yield an extinction-corrected K-band luminosity in a 30″ aperture centered on the nucleus of M82 that is a factor of at least 1.6 smaller than previous values. What effect does this have on the inferred IMF?

In this section, we will treat the integrated properties from a 30″ (450 pc) aperture centered on the nucleus as a single starburst population. We have shown that there is actually an age dispersion among the stellar populations within this aperture. It is therefore a crude approximation to treat the entire starburst region as a single instantaneous burst characterized by a single age; this analysis is intended only to illustrate the relationship between the observed quantities and the parameters derived for the IMF, with an emphasis on testing the validity of a low-mass deficient starburst population in M82. These characteristics are critically dependent on the extinction correction applied to the K-band luminosity and the total mass assumed in the burst. Neither of these quantities is known unequivocally. In order to make firm conclusions about the IMF in the M82 starburst, we stress the importance of interpreting the predictions of these models in the light of the current observational uncertainties.

The extinction-corrected K-band magnitude of M82 has varied widely in the literature. These variations are due to differences in the K-band photometry and to differences in the adopted extinction geometry. Table 4 is a summary of the observed and extinction-corrected (where available) K magnitudes in the literature from a 30″ (450 pc) aperture centered on the nucleus. We have demonstrated in Paper I that our recombination line–derived extinction is the most reliable estimate for the extinction to date toward the central starburst region of M82. We have also shown (see § 4.4) that a slight modification to the foreground screen assumption, a modification that is necessary to explain the corrected colors of the starburst region in terms of the emission from a normal population of stars, does not change substantially the extinction-corrected K-band magnitude. Thus, M_K in a 30″ aperture centered on the nucleus of M82 is very close to our value of -22.0 (Paper I) listed in Table 4.

The total mass involved in the burst is also not determined uniquely. The dynamical mass within the starburst region consists of the total mass of the gas, the total mass of stars involved in the burst, and the mass of stars from an old population of stars predating the burst. There is some observational uncertainty in the estimates for the dynamical mass within the starburst region. There is also a large uncertainty associated with the fraction of this mass that is molecular, and finally the mass of the preexisting stellar population is not known. Hence, there is some flexibility in the mass that can be assigned to the starburst population.

The dynamical mass has been estimated using visible (e.g., Gotz et al. 1990) and mid-infrared emission lines from the ionized gas (e.g., Beck et al. 1978; Achtermann & Lacy 1995), stellar absorption lines (e.g., Gaffney et al. 1993), and molecular lines (Lo et al. 1987, Shen & Lo 1995). These estimates can vary by as much as a factor of 1.5. Table 5 summarizes a selection of these observations. In order to

TABLE 4

SELECTION OF K-BAND MEASUREMENTS

Authors	Observed M_K	Extinction-corrected M_K	Extinction Model
Rieke et al. 1980	...	-23.3	Homogeneous mixture, derived from H recombination lines
Telesco et al. 1991	-22.1	-22.6	Foreground, derived from $H-K$ color
McLeod et al. 1993	...	-22.5	Foreground, derived from $H-K$ color
This work	-21.4	-22.0	Foreground, derived from H recombination lines

TABLE 5

DYNAMICAL MASS ESTIMATES

Authors	Radius (pc)	Mass (10^9 $M_\odot$)	Technique
Shen & Lo 1995	390	2.3	CO (1 → 0) measurements
Achtermann & Lacy 1995	344	1.0	[Ne II] 12.8 μm measurements
Gotz et al. 1990	390	1.5	Na D, Hα, H I 21 cm
	344	1.2	Na D, Hα, H I 21 cm

estimate the mass enclosed in a 30″ aperture ($r = 225$ pc), we use the mass model proposed by Gotz et al. (1990),

$$M(<r) = 5 \times 10^5 r^{1.33} + 4 \times 10^9 \left(\frac{r}{2700}\right)^2 , \qquad (2)$$

where $M(<r)$ is the mass ($M_\odot$) interior to the radius r (pc). Using this model, the mass within a 30″ aperture is 7×10^8 $M_\odot$. This value is the same as that assumed by Rieke et al. (1993).

The molecular gas mass has been estimated using a variety of methods. These methods are summarized by Wild et al. (1992). A selection of these measurements, demonstrating the large discrepancies in the derived molecular masses, is shown in Table 6. It has been shown that the molecular gas conversion factor appropriate for M82 is much smaller than the galactic value (e.g., Lo et al. 1987; Paper I). In addition, we have also shown in Paper I that the geometry of the starburst region can be approximated by a molecular torus surrounding a central cavity containing predominantly ionized gas and stars. Therefore, the estimates for the molecular mass in Table 6 should be much larger than the true value appropriate for the starburst region. Thus, we assume that the central 30″ does not contain more than 10^8 $M_\odot$ of molecular gas, and most probably contains a negligible amount.

The above-mentioned mass constraints and extinction-corrected K-band luminosity can now be applied to our stellar population synthesis models. Using our extinction-corrected absolute K magnitude of -22.0, we find that only 2.5×10^8 $M_\odot$, 36% of the total dynamical mass, is needed in the burst in order to accommodate a Salpeter IMF that extends from 0.1 to 100 $M_\odot$, and that the remaining 3.5×10^8 $M_\odot$, or $\sim$50% of the total dynamical mass, can be locked up in an old population, assuming that the burst age is $\sim 10^7$ yr. The simple modification to the two-screen dust geometry (see § 4.4) gives approximately the same results. In order to illustrate the relationship between M_K, $M_{\rm Tot}$, and m_L, we have taken the range of extinction-corrected K-band magnitudes from Table 4 and calculated the lower mass limit required to produce these magnitudes for a burst age of $\sim 10^7$ yr. Figure 11 is a graph of m_L versus the total mass assumed in the burst, $M_{\rm Tot}$. As can be seen, a moderate variation in the mass allocated to either the burst, shown above to be an uncertain quantity, or the extinction-corrected K flux density—variations that can be tolerated by the current observational constraints—can result in a lower mass cutoff for the starburst region that is much more like the solar neighborhood than has been assumed previously. Note that it has been argued that the actual solar neighborhood IMF is steeper than the Salpeter IMF at high masses (Massey et al. 1995b). However, our assumed IMF does not differ greatly from other assumed IMFs at high masses. If the more recent Miller + Scalo IMF (Miller & Scalo 1979) is assumed instead of the Salpeter IMF, normalizing to the same total mass and assuming the same lower and upper mass cutoffs, the fraction of the total mass in stars with masses greater than 10 $M_\odot$ is 10% compared with 12% for the Salpeter IMF. Thus, a Miller & Scalo

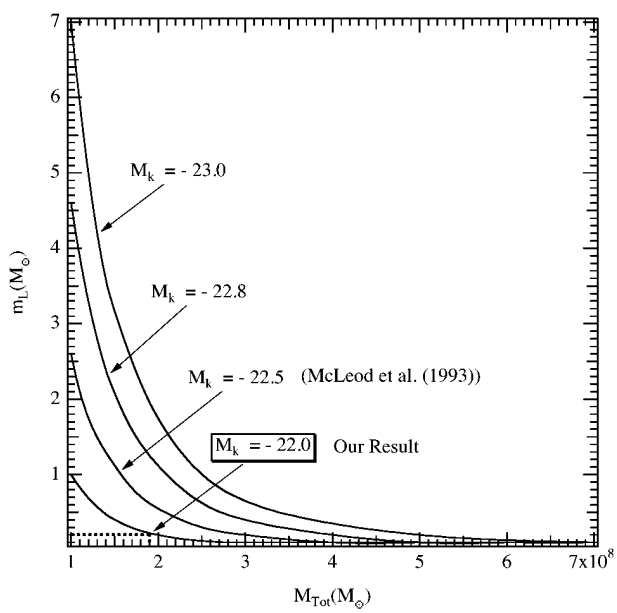

FIG. 11.—Relationship between the lower mass cutoff and the total mass assumed in the burst for various values of the extinction-corrected K magnitudes. The total dynamical mass for the starburst region (450 pc) is 7×10^8 $M_\odot$.

TABLE 6

MOLECULAR MASS ESTIMATES

Authors	Radius (pc)	Mass (10^8 $M_\odot$)	Technique
Wild et al. 1992	800	1.8	$C^{18}O$ (2 → 1)
Carlstrom 1989	375	1.0	CO (1 → 0), assumed optically thin
Lo et al. 1987	700 × 200	0.6	CO (1 → 0), assumed optically thin
Olofsson & Rydbeck 1984	500	0.6	CO (1 → 0), assumed optically thin
Young & Scoville 1984	500	4.0	CO (1 → 0), assumed optically thick
Sutton, Phillips, & Masson 1983	250	0.3	CO (2 → 0), assumed optically thin

IMF extending from 0.1 to 100 $M_\odot$ can replicate the observed extinction-corrected K-band magnitude if the total mass assumed in the burst is increased slightly.

If a large percentage of the total mass is in the form of an old underlying stellar population, the lower mass cutoff required of the burst population becomes greater than 1 $M_\odot$. For example, if we assume that $\sim 70\%$ of the mass is in an old population, the lower mass cutoff required to replicate our observed extinction-corrected K-band magnitude is 1 $M_\odot$. Since it is unknown how much mass is in the form of the underlying stellar population, the possibility that almost all of the mass is in this form, and therefore that the burst population is deficient in low-mass stars, cannot be ruled out. Our model predicts a supernova rate of 0.08–0.1 yr^{-1} for ages between 3×10^6 and 1×10^7 yr when our extinction-corrected K magnitude of -22.0 is matched. This is consistent with estimates derived from radio observations (e.g., 0.1 yr^{-1}, Bartel et al. 1987; 0.05 yr^{-1}, Muxlow et al. 1994). Again, the reader is reminded that the purpose of this discussion is to illustrate primarily the relationship between the various observed quantities and the conclusions regarding the lower mass cutoff of the IMF. In reality, the treatment of the integrated properties from the entire 500 pc as a single instantaneous starburst is, as emphasized in this paper, an oversimplification.

In their most recent work on M82, Rieke et al. (1993), using their updated extinction-corrected K luminosity (McLeod et al. 1993; see Table 4), have modeled the stellar population in a 30″ aperture assuming two Gaussian starbursts, the first to provide the red supergiants and supernovae for the X-ray wind and the second to produce the UV flux (ionizing photon flux). Although their revised extinction-corrected K luminosity is substantially fainter than their 1980 result (Rieke et al. 1980), their conclusion of a low-mass deficient IMF remains unchanged. The crucial factor behind this conclusion is the fact that in their model, they find that at no time do the K and UV luminosities match their observed values. At early times, when the stellar population is dominated by hot young stars and the model UV flux is similar to that observed, the K flux density falls short of its observed value. At later times, when more stars have evolved into supergiants and the K flux density is replicated, the UV flux falls short. Despite their incorporation of two starbursts, either the UV flux or the K flux density falls short by a factor of 2 if a solar neighborhood IMF is assumed and the total mass assumed in the burst is fixed at 2.5×10^8 $M_\odot$. In order to match synchronously these observed quantities without increasing the total mass assumed to be participating in the burst, the IMF needs to suppress the formation of low-mass stars. Part of the complexity of these models arises from the variation in the stellar population within the 450 pc region being modeled. As seen from our Brγ and K images (Paper I), the UV flux is high where the K flux density is low and vice versa. In fact, in a 2″ aperture centered on the nucleus, the ratio of the K flux density to the Brγ flux is a factor of 3 times larger than the ratio in a 30″ aperture. However, the ratio of the dereddened K luminosity to dynamical mass (using eq. [2]) remains the same in these two apertures. A comparison of the more reliable mass estimates derived from near-infrared absorption features with those derived from the ionized gas emission lines shows that L_K/M is even smaller in the central few arcseconds of M82 than in the starburst disk (Gaffney et al. 1993). Thus, a solar neighborhood IMF that includes low-mass stars could be completely consistent with observations if the region modeled were smaller in extent.

7. SUMMARY AND CONCLUSIONS

In this paper, we have compared a starburst stellar population model with a series of detailed high spatial resolution imaging observations described in depth in Paper I. Unlike most previous studies of M82, our data have allowed us to identify and model the properties of the individual stellar clusters in the central 500 pc. In addition to our published near-infrared hydrogen recombination line imaging, near-infrared broadband imaging, and 3.29 μm dust feature imaging observations (Paper I), we have also carried out imaging observations in the 2.36 μm CO band head. Our major results are summarized as follows:

1. The CO 2.36 μm absorption feature is seen to be anticorrelated with the Brγ emission. The CO index is found to be 0.22 at the nucleus of M82, higher than that of normal galaxies (F78). Smaller values are seen farther from the nucleus, suggesting, along with other star formation diagnostics, that the nucleus contains an older population of stars and that the starburst is propagating outward.
2. A comparison of our model quantities with observations allows us to determine the variation in age within the starburst complex. Our analysis implies that the typical age for the starburst clusters is 10^7 yr. The inferred age dispersion between the stellar clusters in the central 500 pc is found to be 6×10^6 yr. If the starburst in M82 is propagating outward from the center, this corresponds to a velocity of propagation, originating in the center, of ~ 50 km s^{-1}.
3. An analysis of the integrated properties in a 30″ aperture ($r = 225$ pc) reveals that our extinction-corrected K magnitude of -22.0 can be accommodated by a Salpeter IMF extending between 0.1 and 100 $M_\odot$ if we assume that 36% of the total dynamical mass within the central 450 pc is in the burst population, leaving more than 50% of the mass for a preexisting population. Our high-resolution data reveal that when the region modeled is decreased in extent, the higher mass–to–K luminosity ratio and the smaller UV photon flux make it increasingly easier to match synchronously the observed properties without invoking a high-mass–biased IMF.

We would like to express our thanks to Kevin McFadden, Jim Cole, Mark Whitis, and Tracy Hodge for their help with the software development, instrument setup, and telescope operation, and Larry Helfer and Mark Wardle for many useful discussions. We are also very grateful to Claus Leitherer for providing electronic versions of all of the figures in his paper and for running his programs for us without including the effects of the nebular continuum so that they could be readily compared with our models. We would also like to thank Daniel Schaerer for sending electronic versions of the stellar tracks. We are also grateful for the many useful comments from the referee. George Rieke also provided us with very insightful and helpful comments. This work was supported in part by the Smithsonian Institution Scholarly Studies Program, NSF grants AST 89-57238, AST 93-57392, AST 91-16644, AST 94-53354, and AST 91-07769, National Geographic Society grant 5077-93, the Office of Naval Research, and the Office of Research, University of Wyoming.

REFERENCES

Aaronson, M. 1977, Ph.D. thesis, Harvard Univ.
Achtermann, J. M., & Lacy, J. H. 1995, ApJ, 439, 163
Bartel, N., et al. 1987, ApJ, 323, 505
Beck, S. C., Lacy, J. H., Baas, F., & Townes, C. H. 1978, ApJ, 226, 545
Bessell, M. S., & Stringfellow, G. S. 1993, ARA&A, 31, 433
Carlstrom, J. E. 1989, Ph.D. dissertation, Univ. California, Berkeley
Carlstrom, J. E., & Kronberg, P. P. 1991, ApJ, 366, 422
Charlot, S., & Bruzual, A. G. 1991, ApJ, 367, 126
Devereux, N. A., Becklin, E. E., & Scoville, N. 1987, ApJ, 312, 529
Doyon, R., Joseph, R. D., & Wright, G. S. 1994, ApJ, 421, 101
Frogel, J. A., Persson, S. E., Aarson, M., & Matthews, K. 1978, ApJ, 220, 75 (F78)
Frogel, J. A., Persson, S. E., & Cohen, J. G. 1983, ApJS, 53, 713
Gaffney, N. I., Lester, D. F., & Telesco, C. M. 1993, ApJ, 407, 57
Gotz, M., McKeith, C. D., Downes, D., & Greve, A. 1990, A&A, 240, 52
Greenhouse, M. A., et al. 1997, ApJ, 475
Kleinmann, S. G., & Hall, D. N. B. 1986, ApJS, 62, 501
Koornneef, J. 1983, A&A, 128, 84
Landini, M., Natta, A., Oliva, E., Salinari, P., & Moorwood, A. F. M. 1984, A&A, 134, 384
Leitherer, C., & Heckman, T. M. 1995, ApJS, 96, 9
Lester, D. F., Carr, J. S., Joy, M., & Gaffney, N. 1990, ApJ, 352, 544
Lo, K. Y., Cheung, K. W., Masson, C. R., Phillips, T. G., Scott, S. L., & Woody, D. P. 1987, ApJ, 312, 574
Massey, P., Johnson, K. E., & DeGioia-Eastwood, K. 1995a, ApJ, 454, 151
Massey, P., Lang, C. C., DeGioia-Eastwood, K., & Garmany, C. D. 1995b, ApJ, 438, 188
McLeod, K. K., Rieke, G. H., Rieke, M. J., & Kelley, D. M. 1993, ApJ, 412, 111
Miller, G. E., & Scalo, J. M. 1979, ApJS, 41, 513
Muxlow, T. W. B., Pedlar, A., Wilkinson, P. M., Axon, D. J., Sanders, E. M., & de Bruyn, A. G. 1994, MNRAS, 266, 455
Olofsson, H., & Rydbeck, G. 1984, A&A, 136, 170
Panagia, N. 1973, AJ, 78, 929
Pipher, J. L., Moneti, A., Forrest, W. J., Woodward, C. E., & Shure, M. A. 1987, in Proc. Workshop on Ground-Based Astronomical Observations with Infrared Detectors, ed. C. G. Wynn-Williams & E. E. Becklin (Honolulu; Univ. Hawaii Press), 326
Puxley, P. J. 1991, MNRAS, 249, 11P
Rieke, G. H., Lebofsky, M. J., Thompson, R. I., Low, F. J., & Tokunaga, A. T. 1980, ApJ, 238, 24
Rieke, G. H., Loken, K., Rieke, M. J., & Tamblyn, P. 1993, ApJ, 412, 99
Salpeter, E. E. 1955, ApJ, 121, 161
Satyapal, S. 1995, Ph.D. dissertation, Univ. Rochester
Satyapal, S., et al. 1995, ApJ, 448, 611 (Paper I)
Sellgren, K., Werner, M. W., & Dinnerstein, H. L. 1983, ApJ, 271, L13
Schaller, G., Schaerer, D., Meynet, G., & Maeder, A. 1992, A&AS, 96, 269
Shen, J., & Lo, K. Y. 1995, ApJ, 445, L99
Smith, D. A., Herter, T., Haynes, M. P., Beichman, C. A., & Gautier, T. N., III. 1996, ApJS, 104, 217
Stetson, P. B. 1987, PASP, 99, 191
Sutton, E. C., Phillips, T. G., & Masson, C. R. 1983, ApJ, 275, L49
Telesco, C. M., Campins, H., Joy, M., Dietz, K., & Decher, R. 1991, ApJ, 369, 135
Thronson, H. A., Jr., & Greenhouse, M. A. 1988, ApJ, 327, 671
Turner, P. C. 1995, Ph.D. thesis, Univ. Rochester
Wild, W., Harris, A. I., Eckert, A., Genzel, R., Graf, U. U., Jackson, J. M., Russel, A. P. G., & Stutek, J. 1992, A&A, 265, 447
Young, J. S., & Scoville, N. Z. 1984, ApJ, 287, 153